CSF1R Is Required for Differentiation and Migration of Langerhans Cells and Langerhans Cell Histiocytosis

Silvia Lonardi[1], Sara Scutera[2], Sara Licini[1], Luisa Lorenzi[1], Anna Maria Cesinaro[3], Luisa Benerini Gatta[1], Carlotta Castagnoli[4], Daniele Bollero[5], Rosaria Sparti[2], Michela Tomaselli[1], Daniela Medicina[1], Federica Calzetti[6], Marco Antonio Cassatella[6], Fabio Facchetti[1], Tiziana Musso[2], and William Vermi[1,5,7]

ABSTRACT

Langerhans cell histiocytosis (LCH) is a rare disorder characterized by tissue accumulation of $CD1a^+CD207^+$ LCH cells. In LCH, somatic mutations of the $BRAF^{V600E}$ gene have been detected in tissue LCH cells, bone marrow $CD34^+$ hematopoietic stem cells, circulating $CD14^+$ monocytes, and $BDCA1^+$ myeloid dendritic cells (DC). Targeting $BRAF^{V600E}$ in clonal Langerhans cells (LC) and their precursors is a potential treatment option for patients whose tumors have the mutation. The development of mouse macrophages and LCs is regulated by the CSF1 receptor (CSF1R). In patients with diffuse-type tenosynovial giant cell tumors, CSF1R inhibition depletes tumor-associated macrophages (TAM) with therapeutic efficacy; however, CSF1R signaling in LCs and LCH has not been investigated. We found through IHC and flow cytometry that CSF1R is normally expressed on human $CD1a^+CD207^+$ LCs in the epidermis and stratified epithelia. LCs that were differentiated from $CD14^+$ monocytes, $BDCA1^+$ DCs, and $CD34^+$ cord blood progenitors expressed CSF1R that was downregulated upon maturation. Immature LCs migrated toward CSF1, but not IL34. Administration of the c-FMS/CSF1R kinase inhibitors GW2580 and BLZ945 significantly reduced human LC migration. In LCH clinical samples, LCH cells (including $BRAF^{V600E}$ cells) and TAMs retained high expression of CSF1R. We also detected the presence of transcripts for its ligand, CSF1, but not IL34, in all tested LCH cases. CSF1R and CSF1 expression in LCH, and their role in LC migration and differentiation, suggests CSF1R signaling blockade as a candidate rational approach for treatment of LCH, including the $BRAF^{V600E}$ and wild-type forms of the disease.

Introduction

Langerhans cell histiocytosis (LCH) is characterized by tissue accumulation of transformed cells with features of Langerhans cells (LC; ref. 1). LCH occurs in children and adults, and ranges from a single-site lesion to systemic forms (2). The diagnosis is based on radiological presentation combined with tissue infiltration of LCs identified by CD1a, CD207, and S100 protein. MAPK activation is recurrent in LCH due to somatic mutations of components of the pathway (3). The identification of $BRAF^{V600E}$ with a mutation-specific antibody allows the confirmation of the clonal identity of most tissue-infiltrating LCs in LCH (4). $BRAF^{V600E}$ is also detected in $CD34^+$ hematopoietic progenitors, circulating $CD11c^+CD14^+$ precursors (5, 6), $BDCA1^+$ myeloid dendritic cells (DC), and $CD16^+$ nonclassical monocytes, suggesting the presence of *BRAF*-mutated LCH cases within the group of myeloid neoplasia (5, 6).

This new paradigm shift in the LCH pathogenesis predicts that clonal circulating precursors are driven to terminal LCs' differentiation by the tissue cytokine milieu. In this context, CSF1 receptor (CSF1R) signaling via its cognate ligands CSF1 and IL34 plays a relevant role in various biological processes leading to differentiation of monocyte-derived cells, particularly macrophages. Accordingly, CSF1R blockade has been proposed (7) as a therapeutic strategy in various cancers, with more than 20 recruiting clinical trials existing (https://clinicaltrials.gov/ct2/results?recrs=ab&cond=Cancer&term=csf1r&cntry=&state=&city=&dist=) that employ this strategy. Among available compounds, the RG7155/emactuzumab, a specific CSF1R-humanized antibody, has been shown to deplete CSF1R-expressing tumor-associated macrophages (TAM) in patients with advanced cancer (7). In addition to macrophages, RG7155/emactuzumab depletes blood $CD16^+$, but not $CD14^+$, monocytes (7), which is consistent with their higher expression of surface CSF1R (7, 8).

Although the role of CSF1 in human DCs has been partially characterized (9, 10), the effects of CSF1R blockade on DC subsets are poorly understood. In mice, LCs are tightly dependent on CSF1R signaling for their development and maintenance (9). Mouse CSF1R binds CSF1 and IL34, the latter being able to promote LC differentiation and maintenance in adulthood (10, 11). In humans, CSF1R is expressed on DC progenitors and monocyte-derived DCs (8, 12, 13), whereas circulating and tissue conventional myeloid DCs are negative for CSF1R expression (8, 14) and are not dependent on CSF1R for their development (15). High serum concentration of CSF1 has been detected in LCH, particularly in the systemic forms (16, 17). In addition, activating mutations in CSF1R have been identified in histiocytic neoplasm (18). However, CSF1R expression and signaling involvement in human LCs and LCH has not been addressed.

[1]Department of Molecular and Translational Medicine, University of Brescia, Brescia, Italy. [2]Department of Public Health and Pediatric Sciences, University of Turin, Turin, Italy. [3]Department of Anatomic Pathology, Modena University Hospital, Modena, Italy. [4]Skin Bank, Department of General and Specialized Surgery, A.O.U. Città della Salute e della Scienza, Turin, Italy. [5]Division of Plastic and Reconstructive Surgery and Burn Center, Department of Surgery, A.O.U. Città della Salute, CTO Hospital, Turin, Italy. [6]Section of General Pathology, Department of Medicine, University of Verona, Verona, Italy. [7]Department of Pathology and Immunology, Washington University, Saint Louis, Missouri.

Note: Supplementary data for this article are available at Cancer Immunology Research Online (http://cancerimmunolres.aacrjournals.org/).

S. Lonardi and S. Scutera contributed equally to this article.

Corresponding Author: William Vermi, University of Brescia, 25123 Brescia, Italy. Phone: 39-030399-8425; Fax: 39-030399-5377; E-mail: william.vermi@unibs.it

Cancer Immunol Res 2020;8:829–41

doi: 10.1158/2326-6066.CIR-19-0232

In this study, we found that CSF1R was expressed in immature human CD207$^+$ LCs, whereas it was lost upon LC maturation, as well as in nodal interdigitating DCs (IDC). CSF1R engaged by CSF1, but not IL34, provided an effective chemotactic signal to LCs. In addition, CSF1R blockade impaired LC differentiation from hematopoietic precursors. LCH cells and TAMs retained CSF1R, as verified in clinical samples. Together, these findings suggest CSF1R blockade as a candidate for the treatment of LCH.

Materials and Methods

Tissue and IHC

Formalin-fixed paraffin-embedded (FFPE) tissue blocks from normal skin ($n = 5$), lung ($n = 2$), esophagus ($n = 2$), cervix ($n = 2$), tonsils ($n = 2$), reactive lymph nodes ($n = 2$), dermatopathic lymphadenitis ($n = 12$), as well as pathologic tissues including LCH ($n = 54$), cutaneous squamous cells carcinoma ($n = 5$), primary cutaneous melanoma ($n = 9$), and mycosis fungoides ($n = 3$) were used. Cases were retrieved from the tissue archive of the Department of Pathology, ASST Spedali Civili di Brescia (Italy) and from Azienda Ospedaliero Universitaria, Modena (Italy). LCH cases inclusion criteria were expression of CD207 and CD1a in the majority of neoplastic cells. The study has been conducted according to the Declaration of Helsinki and approved by the local ethic board (NP906-WV-IMMUNOCAN-CERhum). Four-micrometer-thick tissue sections were used for IHC staining. IHC was performed after appropriate antigen retrieval (40′ in thermostatic waterbath in EDTA buffer pH 8.0 for CSF1R and BDCA1) using antibodies reported in Supplementary Table S1. Single immune reactions were developed using Novolink Polymer Detection System (cat. no. RE7280-K, Leica Biosystems). For double/triple IHC, the second immune reaction was visualized using Mach 4 Universal AP-Polymer Kit (cat. no. M4U536L, Biocare Medical) followed by Ferangi Blue (cat. no. FB813S, Biocare Medical); sequentially, the third immune reaction was visualized using Dako REAL Detection System, Alkaline Phosphatase/RED (cat. no. K5005, Dako). BRAF (VE1) was stained by BenchMark ULTRA IHC/ISH system (cat. no 05342716001, Roche Diagnostics).

LC purification from human skin

Primary LCs and dermal DCs were purified from normal human skin ($n = 10$) obtained as discarded material from reduction abdominoplasty after written consent, according to a protocol approved by the CTO/Città della Salute e della Scienza Hospital Ethical Board (Torino, Italy) and in adherence with the Declaration of Helsinki principles. Following excision of subcutaneous fat, skin was cut in strips and exposed to dispase. Briefly, the skin was digested with 1 U/mL dispase (cat. no. 17105041, Thermo Fisher Scientific) and penicillin–streptomycin solution overnight at 37°C, and the epidermis was peeled off the dermis. Dermal and epidermal sheets were then incubated separately in media containing 1% FBS (cat. no. 10270-106, Thermo Fisher Scientific), 200 U/mL collagenase (cat. no. C5138), and 100 U/mL DNase I (cat. no. 10104159001; Sigma-Aldrich) at 37°C in a rotator for 30 minutes and 2 hours, respectively. The cells were then separated using a tea strainer (700 μm mesh size), and the supernatants were then passed through a 100 μm cell strainer for 2 times. For epidermal suspension, cells were spun at 400 × *g* for 30 minutes on a Ficoll-Paque PLUS (cat. no. GE17-1440-02, GE Healthcare Bio-Sciences, Sigma-Aldrich) gradient, and the immune cells were harvested. Dermal cells were enriched for CD45-expressing cells using magnetic beads (cat. no. 130-045-801, Miltenyi). Cells were then counted and labeled for flow cytometric evaluation of surface expression markers. In some experiments, cells enriched for CD45 (containing LCs) from the epidermis were left untreated or stimulated for 48 hours with LPS (1 μg/mL) and R848 (5 μg/mL).

LC generation

Buffy coats were obtained from healthy blood donors (CPVE-S. Anna, Turin, Italy). Peripheral blood mononuclear cells (PBMC) enriched by Ficoll and CD14$^+$ monocytes and BDCA1$^+$ DCs isolated using anti–CD14-coated beads and human BDCA1$^+$ DC Isolation Kit (cat. no. 130-090-506, Miltenyi). To obtain LC-like DCs, CD14$^+$ monocytes were cultured for 7 days into in RPMI 1640 (cat. no. 21875034, Thermo Fisher Scientific) with 10% FCS (cat. no. 10270-106, Thermo Fisher Scientific) supplemented with GM-CSF (200 ng/mL, cat. no. 300-03), IL4 (20 ng/mL, cat. no. 200-04), and TGFβ (10 ng/mL, cat. no. 100-21C; all from PeproTech; referred to as monocyte-derived LCs; mo-LCs). BDCA1$^+$ DCs were differentiated for 3 days with GM-CSF (100 ng/mL) and TGFβ (10 ng/mL, referred as BDCA1$^+$ LCs). When required, LC-like DCs were matured with LPS (100 ng/mL, cat.no. L4391, Sigma-Aldrich) and R848 (1 μg/mL, cat. no. tlrl-r848, InvivoGen). Cord blood was obtained from Banca del Sangue Placentare following informed consent. CD34$^+$ progenitors were purified from cord blood with CD34 magnetic beads (cat. no. 130-100-453, Miltenyi) and cultured to induce LC-like cells (referred as CD34$^+$-LCs) in X-VIVO 15 media (cat. no.04-448Q, Lonza) with GM-CSF (100 ng/mL), SCF (20 ng/mL, cat. no. 300-07), Flt3 (100 ng/mL, cat. no. 300-19), TNFα (2.5 ng/mL, cat. no. 300-01A), and TGFβ1 (5 ng/mL; all from PeproTech) for 10 days. In differentiation experiments, cells were cultured with CSF1 (100 ng/mL, cat. no. 300-25) or GM-CSF in combination with the other cytokines for respectively 14 and 10 days. In some experiments, CD34$^+$ cells were cultured with GM-CSF or CSF1 in combination with the other cytokines for 12 and 22 days. Cells were differentiated in the absence or presence of BLZ945 (0.5 μmol/L, cat. no. S7725; Selleckchem) added after 7 days.

Flow cytometry

In vitro–differentiated LCs were stained using antibodies detailed in Supplementary Table S1 and analyzed using BD FACSCalibur (BD Biosciences). For dermal and epidermal DCs, cells were stained with antibodies indicated in Supplementary Table S1. Viability was assessed with Viability 405/520 Fixable Dye (cat. no. 130-109-814, Miltenyi) diluted 1:100 or with LIVE/DEAD Violet Viability dye (cat. no. L34955, Thermo Fisher Scientific) diluted 1:1,000.

To minimize FcR-mediated mAb binding, cells were stained in the presence of human serum containing IgG (cat. no. I2511, Sigma-Aldrich) and Tandem Signal Enhancer (cat. no. 130-099-888, Miltenyi) to reduce nonspecific binding of tandem dye–conjugated antibodies to human cells. Briefly cells (1×10^6) were washed in buffer containing PBS pH 7.2, 0.5% BSA, and 2 mmol/L EDTA and stained for viability and blocking before specific antibody staining (incubated for 15 minutes in the dark in the refrigerator). Cells were then washed and fixed in 1% paraformaldehyde and acquired using MACSQuant (Miltenyi) or BD FACSVerseTM (BD Biosciences). Analysis was performed with FlowLogic software.

Cell sorting for preparation of cell blocks

Fresh PBMCs were isolated from buffy coat of healthy donors by density centrifugation using Ficoll-Paque gradient (GE Healthcare). For purification of monocytes populations and BDCA1$^+$ DCs, PBMCs were stained with the following panel of human antibodies: FITC-CD14 (clone TUK4, cat. no. 130-113-146, Miltenyi), PE-CD56 (clone AF12-7H3, cat. no. 130-090-755, Miltenyi), perCP-Cy5.5–

CD16 (clone 3G8, cat. no. 302030 Biolegend), PE-VIO770–CD3 (clone REA613, cat. no. 130-113-140, Miltenyi), PE-VIO770 CD20 (clone LT20, cat. no. 130-113-375, Miltenyi), APC-CD303 (clone AC144, cat. no. 130-090-905, Miltenyi), APC-CD141 (clone AD5-14H12, cat. no. 130-113-314, Miltenyi), and APC-Cy7–HLA-DR (clone L243, cat. no. 307618, Biolegend) and sorted using FACSAria II (BD Biosciences). Accordingly, PBMCs were subjected to doublets exclusion and subsequently gated on lymphocytes negative (CD3, CD19, and CD56) and HLA-DR–positive cells, and finally monocytes were positively selected as $CD14^+CD16^-$ or $CD14^-CD16^+$, whereas $BDCA1^+$ were negatively selected as $CD14^-CD16^-CD141^-$ and $CD303^-$. Fluorescence negative controls were performed using intra-simple-negative populations as reference.

For cell block preparation, cell suspensions of sorted cells were centrifuged for 10 minutes at 3,000 rpm. A solution of plasma (100 mL, kindly provided by Centro Trasfusionale, ASST Spedali Civili) and HemosIL RecombiPlasTin 2G (200 mL, Instrumentation Laboratory; cat. no. 0020003050; 1:2) was added to cell pellets, mixed until the formation of a clot, then placed into a bio-cassette (Bio-Optica; cat. no. 07-7350). The specimen was fixed in 10% formalin (Bio-Optica; cat. no. 05-K01004) for 1 hour followed by paraffin inclusion.

LC migration assay

Migration of mo-LCs was measured in triplicate with a transwell system (cat. no.3421, 24-well plates; 5.0 μm pore size; Corning Costar). RPMI 1640 with 1% FCS alone, with varying doses of CSF1 or IL34 (cat. no. 200-34, PeproTech), was added to the lower chamber. Wells with medium alone were used as a control for spontaneous migration. A total of 2.5×105 cells in 200 μL were added to the upper chamber and incubated at 37°C for 4 hours. In some migration experiments, cells were pretreated with GW2580 (1 μmol/L, cat. no. SML1047, Sigma-Aldrich) or BLZ945 (0.5 μmol/L, Selleckchem) for 60 minutes at 37°C. For migration of $BDCA1^+$ LCs, 1.5×105 cells in 200 μL were added to the upper chamber of a transwell system (5.0 μm pore size; Corning Costar) and harvested after 6 hours of migration toward CSF1 (50 ng/mL). Mo-LCs and $BDCA1^+$ LCs were not enriched for CD207. Cells migrated into the lower chamber were harvested, concentrated to a volume of 300 μL of PBS, and counted by flow cytometry. Events were acquired for a fixed time of 60 seconds. The counts fell within a linear range of the control titration curves obtained by testing increasing cell concentrations. Values are given as the mean number of migrated cells ± SEM.

Apoptosis assay

Mo-LCs were incubated in RPMI 10% FCS for 48 hours in the presence or absence of CSF1 or IL34 (50 ng/mL), to evaluate their capacity of protection. Cells were washed, resuspended in Annexin Buffer, and evaluated for apoptosis using the Annexin V–FITC apoptosis detection kit (cat. no. 640914, Biolegend).

BRAF genotyping by digital PCR

DNA of 20 LCH cases (details in Supplementary Table S2) was extracted from sections of archival paraffin blocks using the QIAamp DNA FFPE Tissue Kit (cat. no. 56404, QIAGEN). QX200 Droplet Digital PCR system (Bio-Rad) was used for analysis of $BRAF^{V600E}$ mutation. Digital droplet PCR (ddPCR) reagents were purchased from Bio-Rad and included the ddPCR Mutation Assay *BRAF* V600E FAM/HEX. $BRAF^{V600E}$ cutaneous melanomas were included as positive control sample. The droplet emulsions were thermally cycled with the use of the following protocol: denaturation at 95°C for 10 minutes, followed by 40 cycles of 94°C for 30 seconds and 55°C for 1 minute. After cycling, a final 10-minute hold at 98°C was applied to deactivate the enzyme and to stabilize the droplets. Experiments have been performed in duplicate.

Gene expression profile by ddPCR

Expression profile for selected targets was performed by ddPCR using the Bio-Rad QX200 ddPCR platform. Briefly, RNA of 12 LCH cases from skin, lung, bone, and lymph node (#6, #13, #16, #19, #31, #35, #40, #44, #45, #47, #50, #51; see Supplementary Table S2 for details) was extracted from sections using the RNeasy FFPE Kit (cat. no. 73504, QIAGEN). The cDNAs were synthesized from total RNA using the iScript gDNA Clear cDNA Synthesis Kit (cat. no. 1725035, Bio-Rad), in a volume of 20 μL, prior to droplet formation. The RNA expression for all targets was normalized to UBC expression. The human PrimePCR ddPCR Expression Probe Assays (Bio-Rad) were used at a final concentration of 1X and include KRT14 dHsaCPE5192231, CSF1R dHsaCPE5042034, CSF1 dHsaCPE5042260, IL-34 dHsaCPE5038840, CD207 dHsaCPE5035151, and UBC dHsaCPE5190156. All assays were analyzed using QuantaSoft Software (Bio-Rad).

Statistical analysis

Statistical significance was determined by using nonparametric Student *t* test or ANOVA followed by Tukey Multiple Comparison test, as appropriate. Results were analyzed by using GraphPad PRISM5.0 software.

Results

CSF1R expression in human intraepithelial LCs and tumor-associated LCs

We tested CSF1R expression on human tissues by using a CSF1R antibody (clone FER216) that recognizes CSF1R on $CD16^+$ and $CD14^+$ circulating monocytes (7, 8) from cell block preparations (Supplementary Fig. S1A), $CD68^+$ macrophages in reactive lymph nodes, and TAMs in human lymphomas, but that results negative on most lymphoid cells (19). In normal skin ($n = 2$), tonsil ($n = 2$), lung ($n = 2$), esophagus ($n = 2$), and uterine cervix ($n = 2$), most of the $CD1a^+CD207^+$ LCs within the epithelium express CSF1R (**Fig. 1A–C**; Supplementary Fig. S1B–S1D). Moreover, macrophages in all of these tissues reacted to anti-CSF1R, as confirmed by coexpression of CD163 (**Fig. 1D**), whereas no reactivity could be detected by using an isotype control (Supplementary Fig. S1E).

Dermal DCs in noninflamed normal skin are typically sparse. We could expand the analysis in FFPE samples containing a sizeable number of dermal immune cells by measuring cDC1s ($CD141^+$), cDC2s ($BDCA1/CD1c^+$), and the previously identified dermal $CD207^+$ DC subset (12). We validated a BDCA1 antibody for FFPE using cell block preparations of peripheral blood $BDCA1^+$ DCs (Supplementary Fig. S1F). By using a set of markers including CD1a, BDCA1, CD207, and IRF4, we found that most dermal myeloid DCs were negative for CSF1R (**Fig. 1E–G**). This combination of antibodies confirmed the non-LC identity of the small fraction of $CD207^+$ dermal cells, as suggested by others (12). $CD207^+$ dermal DCs reacted to BDCA1 (**Fig. 1H**) and expressed IRF4, a cDC2 transcription factor (**Fig. 1I**) that is typically negative on LCs (**Fig. 1I**, top right). Our findings confirm a distinct cDC2 phenotype of $CD207^+$ dermal DCs in human tissue. Consistent with the IHC results, flow cytometry analysis of human epidermal cell suspensions revealed CSF1R expression on LCs, the latter populations defined as $CD1a^+CD207^+$ cells

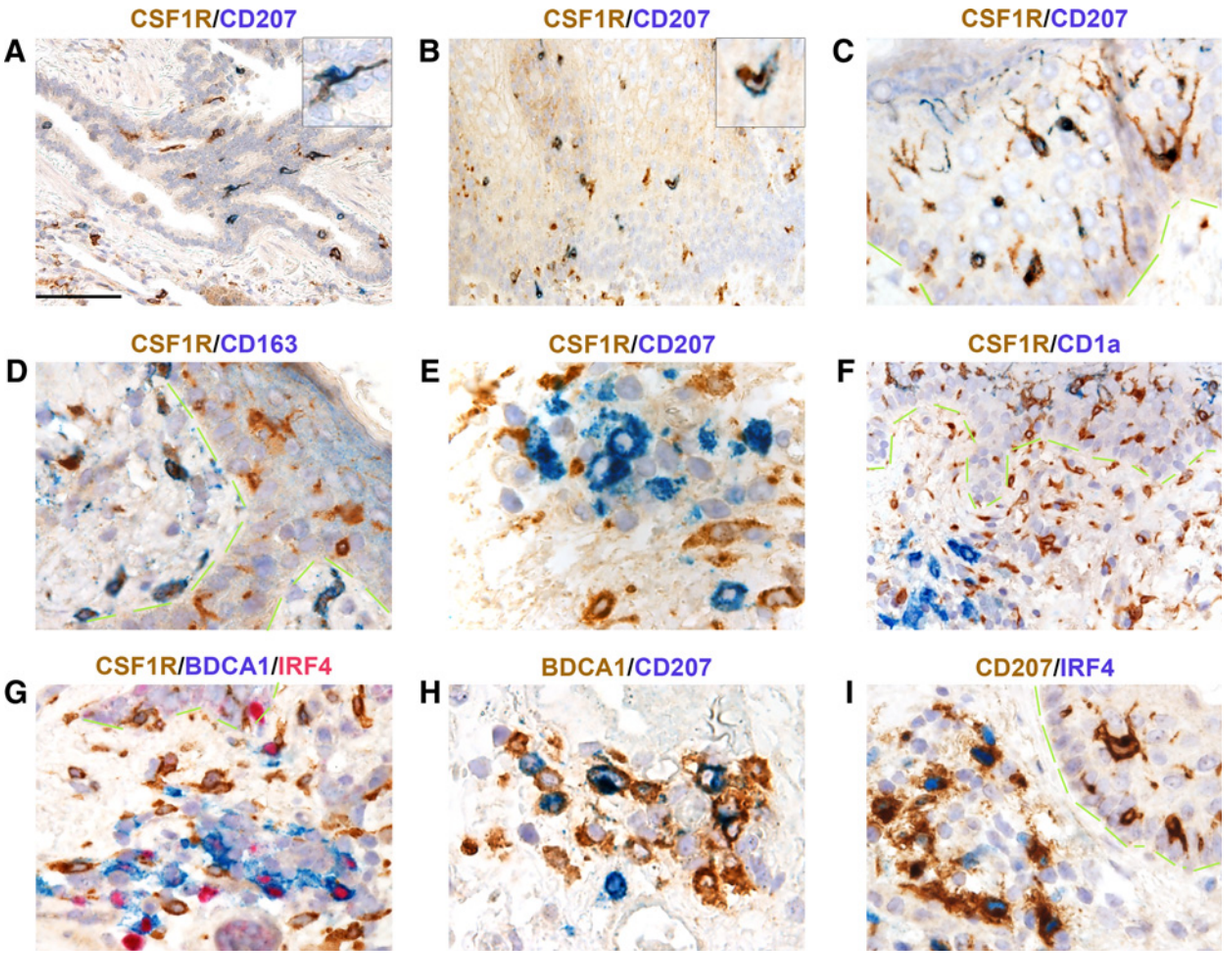

Figure 1.

CSF1R recognizes CD207$^+$ LCs but not dermal CD207$^+$ DCs. Sections are from reactive human lung (**A**), esophagus (**B**), and skin (**C–I**) and stained as labeled. CD207$^+$ LCs in bronchus epithelium (**A**), esophagus mucosa (**B**), and normal skin (**C**) coexpress CSF1R. Dermal CSF1R$^+$ cells largely correspond to CD163$^+$ macrophages (**D**). CSF1R is mainly negative in CD207$^+$ (**E**), CD1a$^+$ (**F**), and BDCA1$^+$ (**G**) dermal DCs. Dermal CD207$^+$ DCs are mostly BDCA1$^+$ (**H**) and IRF4$^+$ (**I**). Green traces separate epidermis from dermis. Sections are counterstained with hematoxylin. Original magnification, 200x (**A**, **B**, and **F**: scale bar, 100 μm), 400x (**C**, **D**, **G**, and **I**: scale bar, 50 μm), and 600x (**E** and **H**: scale bar, 33 μm). Insets were obtained by single cell resizing of a 200x magnification. Microphotographs were taken using the acquisition software cellSens (Olympus) and DP-73 Olympus digital camera mounted on the Olympus BX60 microscope.

within the CD45$^+$HLA-DR^{++} fraction (**Fig. 2A**; Supplementary Fig. S2A). As compared with freshly isolated LCs (**Fig. 2A**), a decrease in CSF1R expression on CD1a$^+$CD207$^+$ cells was observed after 48 hours in epidermal CD45-enriched cell culture in the absence (14% reduction respect to freshly isolated cells) or, even more so, in the presence of stimulation with LPS and R848 (12% reduction respect to unstimulated cells; **Fig. 2B**), indicating that CSF1R is downregulated during LC maturation. Analysis on dermal cell suspensions revealed a low expression of CSF1R on the CD1a$^+$CD207$^-$ (about 6%) and on the CD1a$^+$CD207$^+$ (about 2%) DCs; in contrast, a higher percentage of CSF1R$^+$ cells was observed in the CD1a$^-$ fraction, likely corresponding to monocytes and dermal macrophages (Supplementary Fig. S2B).

CD207$^+$ tumor–associated LCs have been reported in various cutaneous cancers (20). We further expanded our analysis on cutaneous tumor-associated CD207$^+$ cells. We analyzed cutaneous melanomas ($n = 9$), squamous cell carcinomas ($n = 5$), and mycoses fungoides ($n = 3$), and found that CD207$^+$CSF1R$^+$ cells were mainly confined to the intraepithelial compartment, whereas dermal CD207$^+$ cells largely lacked expression of CSF1R (Supplementary Fig. S3) and coexpressed the cDC2 markers IRF4 and BDCA1 (Supplementary Fig. S3B, S3C, S3E, and S3F).

Altogether, these findings establish that CSF1R is expressed in intraepithelial CD207$^+$ LCs but not in CD207$^+$ cDC2. This profile is similar in skin cancers.

CSF1R modulation during LC differentiation and maturation

LCs can be differentiated from monocytes or CD34$^+$ progenitor cells. In addition, circulating BDCA1$^+$ DCs are identified as an alternative source of LC precursors (12, 21). LCH cells are presumed to arise from clonal BDCA1$^+$ DC precursors (22). We thus evaluated CSF1R expression on LCs obtained from different precursors. Surface CSF1R expression was found on about 60% of mo-LCs ($n = 6$), as well as on LCs obtained from CD34$^+$ ($n = 4$) and BDCA1$^+$ DC precursors ($n = 5$; **Fig. 3A**). In line with our observation on freshly purified primary LCs (**Fig. 2B**), CSF1R expression was significantly

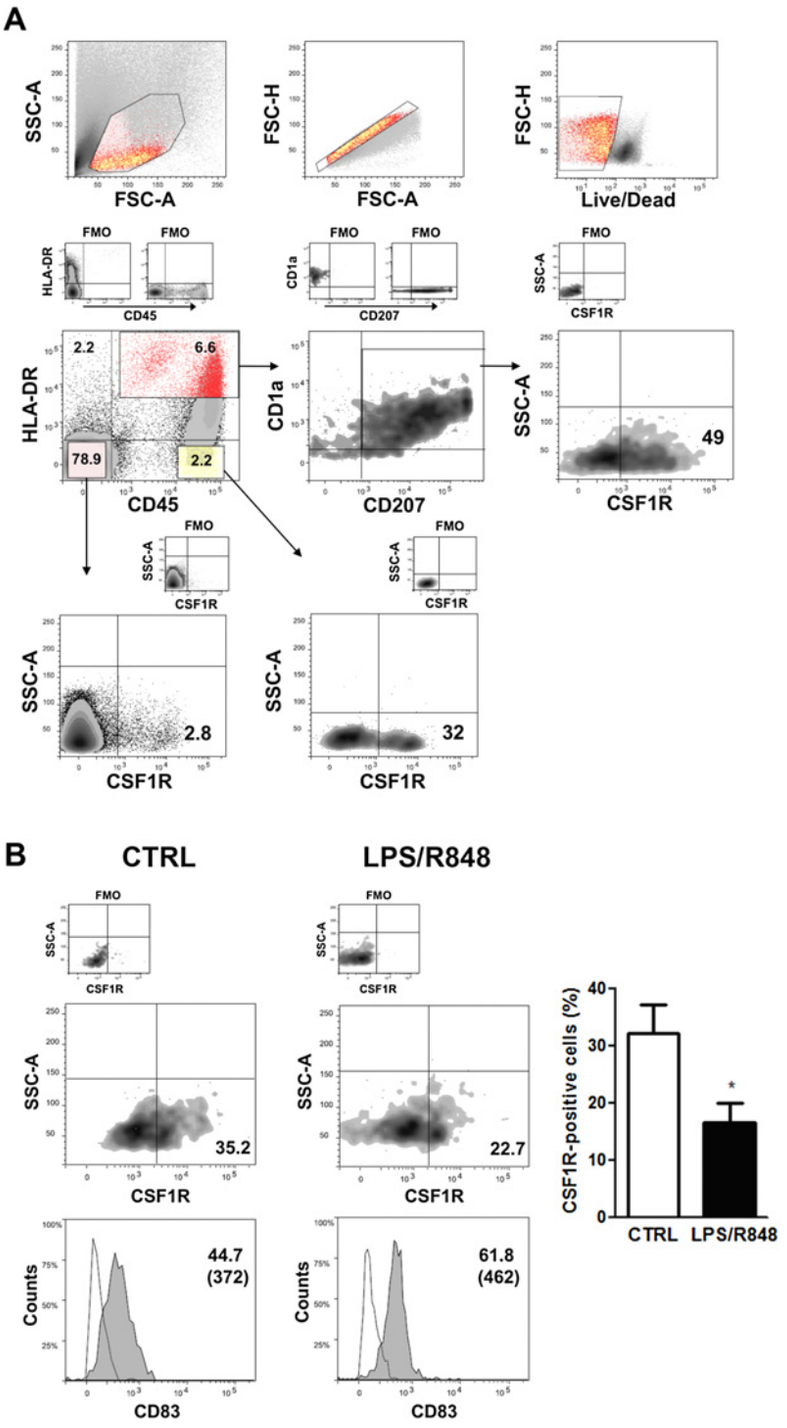

Figure 2.

Expression of CSF1R on human epidermal subpopulations. **A,** Single-cell suspensions from human epidermis were processed for flow cytometry analysis. Gating strategy used to exclude cell debris, doublets, and dead cells is presented in the plot. CSF1R surface expression was analyzed in the $CD1a^+CD207^+$ fraction within the $CD45^+$ $HLA\text{-}DR^{++}$ population (red). In parallel, expression of CSF1R was verified in $CD45^-$ (pink) and $CD45^+$ (yellow) cells. Fluorescence minus one (FMO) controls for the antibodies are shown. Data from one representative experiment are presented ($n = 5$). **B,** $CD45^+$ epidermal cells were untreated or stimulated for 48 hours with LPS (1 μg/mL) and R848 (5 μg/mL) and evaluated for CSF1R and CD83 expression by flow cytometry analysis, using the same gating strategy of **A** (one representative experiment out of four is shown). The values in the bottom graph show the average percentage of $CSF1R^+$ cells ± SEM from four independent experiments. *, $P < 0.05$ versus untreated cells by Student *t* test.

downregulated in mature mo-LCs, in parallel with an upregulation of CD83 and IRF4 expression (**Fig. 3B**).

Nodal LC-like cells are undetectable in unstimulated lymph nodes, but they are easily identifiable within the lymphatic sinuses and in expanded T-cell nodules of the paracortex in the so-called dermatopathic lymphadenitis. This is a condition in which, following proinflammatory stimuli, LCs migrate to draining lymph nodes and undergo maturation. In the paracortex of human lymph nodes, the LC-like population has been referred by pathologists to as IDC and displays the $S100^+CD1a^+CD207^{+/-}$ phenotype. Expectedly, IDCs also coexpress a set of maturation markers such as CD80, CD83, CD208, and CCR7. By evaluating CSF1R expression on ten cases of dermatopathic lymphadenitis, we found CSF1R expression on macrophages in various nodal compartments (Supplementary Fig. S4A), in line with published

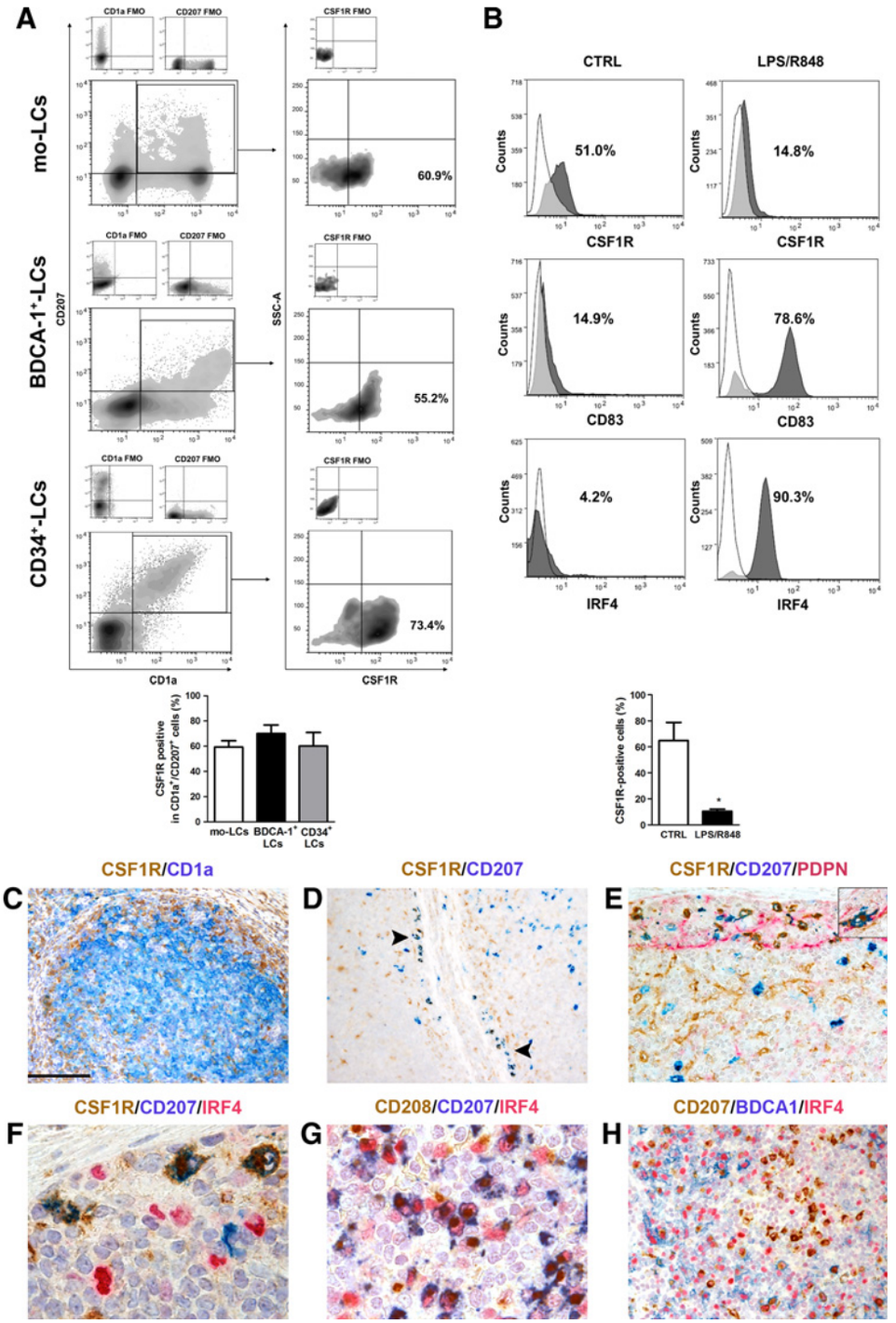

Figure 3.

CSF1R modulation during DC differentiation and maturation. **A,** LCs differentiated from human CD14$^+$ cells (mo-LCs), BDCA1$^+$ cells, and CD34$^+$ cells were evaluated for the expression of CSF1R in the CD1a$^+$CD207$^+$ fraction. Controls for CSF1R (fluorescence minus one, FMO) are shown. Representative flow cytometry analysis (top) and summary results (bottom; mean ± SEM) of, respectively, six (mo-LCs), five (BDCA1$^+$ LCs), and four (CD34$^+$ LCs) experiments are shown. **B,** Mo-LCs were untreated or stimulated for 48 hours with LPS (100 ng/mL) and R848 (1 μg/mL) and evaluated for CSF1R, CD83, and IRF4 expression by FACS analysis (one representative experiment is shown). FMO controls for all antibodies are shown. The values in the bottom graph show the average percentage of CSF1R$^+$ cells ± SEM evaluated in four independent experiments. *, $P < 0.05$ versus untreated LCs by Student t test. Sections are from three human skin-draining lymph nodes with dermatopathic reaction and stained as labeled. CSF1R$^+$ cells are predominantly located at the periphery of dermatopathic CD1a$^+$ nodules (**C**) and within the lymphatic sinus coexpressing CD207 (**D**, black arrows, **E**) but not IRF4 (**F**); sinuses are lined by PDPN$^+$ endothelial cells (**E**). Paracortical IDC nodules are composed by mature CD208$^+$CD207$^+$ IDCs coexpressing IRF4 (**G**). The two IDC populations include CD207$^{+/-}$BDCA1$^+$ cells mainly in the outer paracortex and CD207$^+$BDCA1$^-$ in the inner paracortex (**H**); both populations express IRF4 (**H**). Sections are counterstained with hematoxylin. Original magnification: 100x (**C** and **D**: scale bar, 200 μm), 200x (**E** and **H**: scale bar, 100 μm), and 600x (**F** and **G**: scale bar, 33 μm).

data (19). On the contrary, IDCs of the paracortex largely lacked CSF1R expression (**Fig. 3C** and **D**), although it was possible to identify a small population of CSF1R$^+$CD207$^+$ within the nodal lymphatic sinuses (**Fig. 3D–F**; Supplementary Fig. S4B–S4E).

The notion that IDCs in the paracortex are mainly LC-derived has been challenged, particularly in the mouse system. Cells of non-LC identity and likely corresponding to cDC2s have been identified in the T-cell paracortex (23). By analysis of dermatopathic lymphadenitis ($n = 4$), CSF1R$^+$CD207$^+$ LCs within the nodal lymphatic sinuses lacked expression of BDCA1 and IRF4 (**Fig. 3F**; Supplementary Fig. S4B and S4C) and lacked the maturation markers CD83 and CD208 (Supplementary Fig. S4D and S4E). On the contrary, most IDCs in the paracortical T-cell nodules expressed the transcription factor IRF4 (**Fig. 3G** and **H**). Further, we could identify two main IDC subpopulations showing a distinct localization (**Fig. 3H**; Supplementary Fig. S4F and S4G). Cells in the outer paracortex that coexpressed

BDCA1 and IRF4, and expressed CD83 and CD208, likely correspond to mature cDC2 (**Fig. 3H**; Supplementary Fig. S4G and S4H). Nodal cDC2s can derive from circulating cDC2s via high endothelial venules or from migrating dermal cDC2s, including the $CD207^+$ minor subset. The second subpopulation was mainly located in the inner paracortex and included $CD207^+BDCA1^-IRF4^+$ cells (**Fig. 3H**; Supplementary Fig. S4F and S4G) coexpressing CD208 (Supplementary Fig. S4G), likely corresponding to mature LCs; accordingly, we could demonstrate IRF4 induction upon *in vitro* maturation of LC (**Fig. 3B**). Of note, mouse dermal DCs migrate in the outer paracortex, whereas epidermal LCs are mainly found in the inner paracortical area (24). With some heterogeneity from case to case, we uncovered a third minor fraction of the $BDCA1^+$ in the paracortex coexpressing CD207 (Supplementary Fig. S4G, black arrow); a similar population was also found within the nodal sinuses, likely representing migrating dermal $CD207^+$ cDC2s (Supplementary Fig. S4I). Altogether, these findings suggest that CSF1R expression is tightly associated with LC differentiation but is lost upon maturation. Immature $CSF1R^+$LCs are confined to the nodal sinuses, whereas their maturation is coupled with loss of CSF1R. Moreover, a dermal cDC2 identity of a fraction of $CSF1R^-$ IDCs should be considered.

CSF1R inhibition impairs LC migration and differentiation

CSF1R signaling is relevant during macrophage proliferation and differentiation (25). CSF1R blockade in tumor-bearing mice and patients with cancer results in depletion and molecular reprogramming of TAMs (26). CSF1R-induced cell migration plays an important role in macrophage trafficking to tumor tissues (27). We examined the ability of mo-LCs to migrate toward CSF1 and IL34 ($n = 4$). CSF1 showed a significant chemotactic effect at 50 ng/mL that is maintained at 200 ng/mL (**Fig. 4A**, left; Supplementary Fig. S5A). No effect of IL34 on mo-LCs migration was observed (**Fig. 4A**, left; Supplementary Fig. S5A). The migration toward CSF1 diminished following treatment with the c-FMS/CSF1R kinase inhibitors GW2580 and BLZ945 (**Fig. 4A**, middle). The chemotactic effect of CSF1 was also demonstrated in $BDCA1^+$ DC–derived LCs (**Fig. 4A**, right). Because IL34 and CSF1 have been shown to promote cell survival (28), we investigated the role of these two cytokines in mo-LC viability ($n = 4$). No significant differences were observed in the percentage of live mo-LCs following IL34 and CSF1 treatment compared with untreated cells (Supplementary Fig. S5B). Data on the role of CSF1 on the differentiation of $CD207^+$ cells from precursors are largely missing in the literature. We generated LCs from $CD34^+$ progenitor ($n = 3$) cells in presence of the standard cytokine cocktail (SCF, Flt3L, TNFα, and TGFβ1) in combination with CSF1 and compared with GM-CSF (**Fig. 4B**). CSF1 induced a consistent differentiation in $CD1a^+CD207^+$ cells (88.3±2.7%), and the blockade of the CSF1/CSF1R signaling with BLZ945 significantly reduced differentiation (53 ± 6.7%) of $CD1a^+CD207^+$ cells ($P = 0.0083$). The percentage of $CD1a^+CD207^+$ cells recovered from CSF1 culture was higher than that obtained from GM-CSF culture, and the latter was not affected by BLZ945 (**Fig. 4B**, right; $P = 0.83$). Based on the different kinetics of differentiation between the two experimental conditions (29, 30), the analysis was performed at 10 and 14 days of culture, respectively, for GM-CSF and CSF1. However, the BLZ945 effect on CSF1 but not GM-CSF culture was also confirmed when cells were treated for the same length of time (12 and 22 days; Supplementary Fig. S6). The cell recovery yield was higher for GM-CSF culture compared with CSF1. Specifically, starting from 0.2 × 106 $CD34^+$ cells, the absolute number of viable cells recovered from GM-CSF culture was 11.2 ± 4.8 × 106 (56 ± 24-fold increase), but no differences were observed after BLZ945 treatment ($P = 0.975$). The yield of cells from CSF1 culture was 3.3 ± 0.8 × 106 (17 ± 3.9-fold increase) but was significantly reduced by the addition of BLZ945 ($P = 0.039$).

These results indicate that CSF1 regulates LC migration and may induce LC differentiation from $CD34^+$ precursors.

CSF1R expression in neoplastic cells and TAMs in LCH

Clonally transformed LCs are found in LCH (1). LCH biopsies show tissue infiltration of $CD1a^+CD207^+S100^+$ LCs on a background of inflammatory cells including eosinophils and macrophages. We tested the expression of CSF1R in a large retrospective cohort of LCH biopsies ($n = 54$) including 9 multisystemic disease (**Table 1** and details in Supplementary Table S2). Two representative cases are illustrated in **Fig. 5**. LCH diagnosis was defined based on the morphology and phenotype of LCH cells using CD1a, CD207, and S100 (**Fig. 5A–T**). In addition, LCH cases were tested for $BRAF^{V600E}$ mutation by IHC (**Fig. 5E**, **J**, **O**, and **T**; Supplementary Table S2 and Supplementary Fig. S7) and droplet digital PCR (Supplementary Table S2 and Supplementary Fig. S7E, S7J, and S7O). We found that CSF1R was expressed in all cases (Supplementary Table S2). The stain was observed in the cytoplasm as well as on the cell membrane ($n = 33/54$; 61.1% of LCH cases; **Fig. 5I**; Supplementary Fig. S7C, S7H, and S7M; Supplementary Table S2). CSF1R expression on tissue LCH cells was confirmed in serial sections (Supplementary Fig. S7) and by its colocalization with cytoplasmic anti-VE1, recognizing the $BRAF^{V600E}$ mutant (**Fig. 5U–W**). We could confirm CSF1R reactivity also by using a second antibody (clone SP211, rabbit monoclonal) recognizing a portion of the intracellular domain of CSF1R (Supplementary Fig. S8). In addition to neoplastic cells, anti-CSF1R also reacted with surrounding $CD163^+$ tumor–associated macrophages (**Fig. 5X**).

Based on the downmodulation of CSF1R in matured LCs, we tested the phenotype of neoplastic LCs in a set of LCH cases ($n = 9$). Most neoplastic LCH cells regularly display an immature phenotype, as previously reported (31), largely lacking expression for CD83, CD208, and CCR7 (Supplementary Fig. S7P–S7R). Findings suggest that circulating LCH cells display a cDC2 phenotype and likely represent immediate precursors of transformed LC cells (22). Staining for BDCA1 and CD207 confirms a highly frequent ($n = 43/43$; 100%) and diffuse expression of BDCA1 on tissue $CD207^+$ LCH cells (Supplementary Fig. S7S and S7T). Coexpression of IRF4 with CD207 was frequently observed ($n = 35/46$; 76.1%), although it was highly heterogeneous in its distribution (**Fig. 5Y**; Supplementary Table S2). This hybrid phenotype indicates that, in more than two thirds of the cases, tissue LCH cells are cDC2-derived. However, CSF1R expression in LCH is stably retained irrespectively of their phenotype. In addition, CSF1R expression is also found in surrounding TAMs, indicating that both cell types might be targeted by CSF1R blockade.

CSF1 transcript and phospho-p44/42 expression in LCH tissues

We next analyzed the expression of CSF1, CSF1R, and IL34 in a group of 12 LCH cases, with available archival material including skin and extracutaneous LCH, by ddPCR. Keratin 14 (KRT14) and CD207 were used as markers of epidermal keratinocytes and neoplastic LCH cells. Accordingly, KRT14 transcript expression was limited to skin biopsies, whereas CD207 expression was often found to be comparable in skin and extracutaneous LCH. We could detect expression of CSF1 (10/12; 83.3%) and CSF1R (12/12; 100%) in the large majority of the

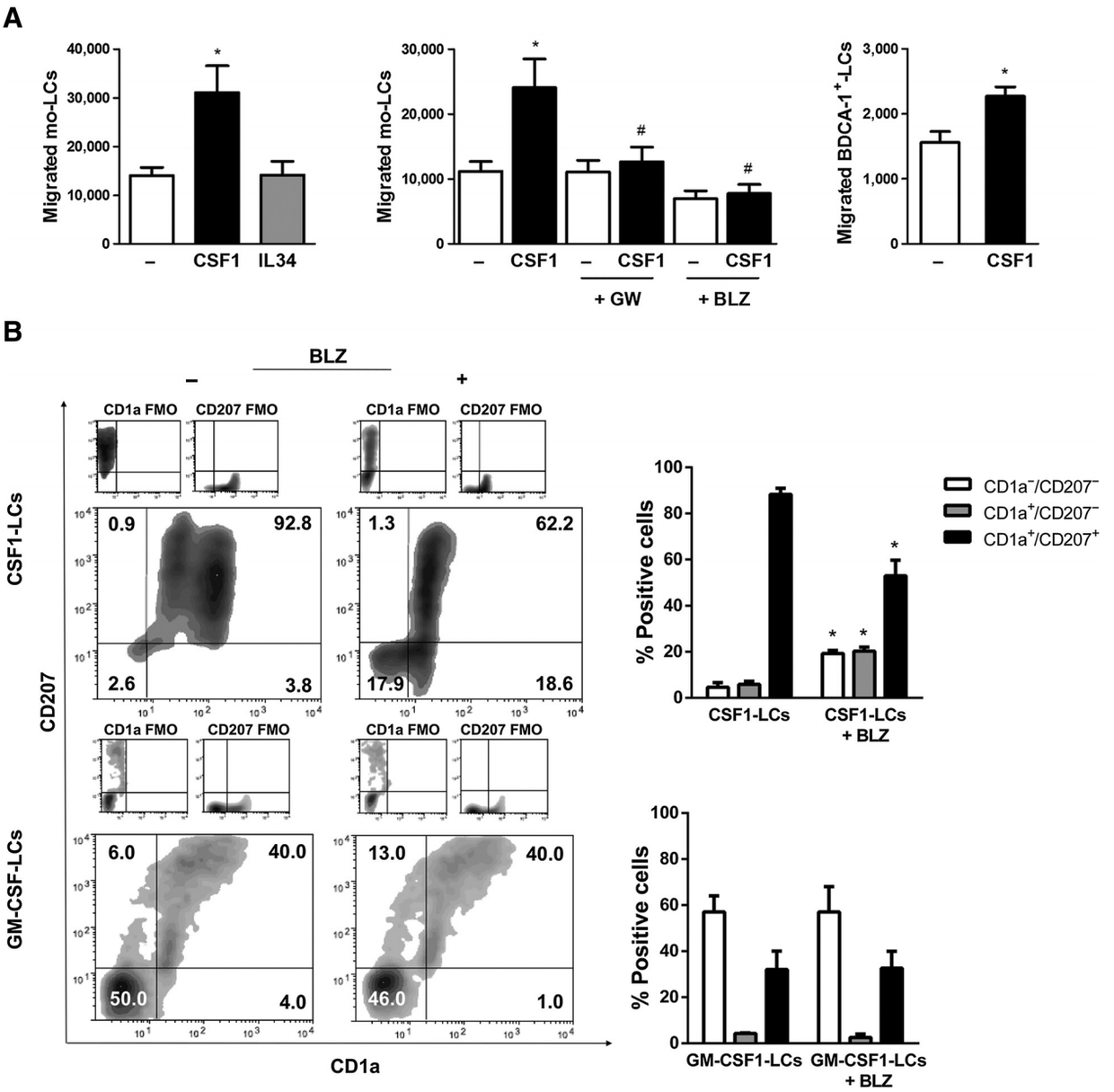

Figure 4.

Effect of CSF1R ligands on LCs. **A,** Mo-LCs (2.5 × 105) were seeded in the upper compartments of a 24-well Transwell cell culture chamber; CSF1 or IL34 (50 ng/mL) were added to the lower compartments. Cells that migrated to the lower compartments after 4-hour incubation were counted by flow cytometry (left). Mo-LCs were preincubated with GW2580 (1 μmol/L) or BLZ945 (0.5 μmol/L) for 1 hour at 37°C. Thereafter, chemotaxis was measured in response to CSF1 (middle). The chemotaxis of BDCA1$^+$ LCs was measured in response to CSF1 (50 ng/mL) after 6-hour incubation (right). Assays were performed in triplicate. Mean value ± SEM of four independent experiments for mo-LCs and of three independent experiments for BDCA1$^+$ LCs are shown. *, $P < 0.05$ versus untreated LCs; #, $P < 0.05$ versus CSF1-migrated LCs by one-way ANOVA, followed by Tukey multiple comparison test or by Student *t* test as appropriate. **B,** LCs were differentiated from CD34$^+$ cells in the presence of CSF1 or GM-CSF for 14 and 10 days, respectively. In parallel, cells were treated with BLZ945 (0.5 μmol/L) for the indicated culture conditions. One representative experiment of the expression of CD1a and CD207 is shown as a flow cytometry dot plot. Fluorescence minus one (FMO) controls for antibodies are shown. The average percentage of CD1a$^-$/CD207$^-$, CD1a$^+$/CD207$^-$, and CD1a$^+$/CD207$^+$ cells within CSF1-differentiated LCs and GM-CSF–differentiated LCs in the presence or absence of BLZ945 is reported (mean value ± SEM of three independent experiments). *, $P < 0.05$ versus untreated LCs by Student *t* test.

LCH cases (**Fig. 6A** and **B**), whereas IL34 expression was largely absent. CSF1R engagement by CSF1 results in downstream activation of the MAPK pathway. Similar to *BRAF*-mutated cases ($n = 8$; Supplementary Fig. S9), in *BRAF* wild-type cases ($n = 6$), CSF1R$^+$ neoplastic cells frequently stained for anti–phospho-p44/42 MAPK (Thr202/Tyr204) as demonstrated in serial sections; anti–phospho-p44/42 was also detected in some TAMs (**Fig. 6C–H**). These findings suggest MAPK pathway activation also occurs in the absence of *BRAF* mutations and might partially rely on CSF1R signaling.

Table 1. Summary of LCH cases analyzed.

Site of LCH lesion	Number of cases	Median age (year range)	Gender (M;F)	*BRAF*^{V600E} (%)	MD (%)
Skin	16	15,4	11;5	8 (36,4)	6 (27,3)
Bone	20	17	13;7	8 (40)	0 (0)
Soft tissue	5	15	1;4	2 (40)	1 (20)
Lung	5	28,8	1;4	4 (80)	0 (0)
Lymph node	4	41,6	2;2	0 (0)	1 (25)
Other localization	4	17,25	2;2	3 (75)	1 (25)
Total	54	22,5 (1 day–79 years)	30;24	25 (41,7)	9 (15)

Abbreviations: MD, multisystemic disease; M;F, male;female.

Discussion

LCs are specialized DCs located within the epithelial surface. During inflammation, LCs can arise from CD34$^+$ progenitors, classical monocytes, and BDCA1$^+$ blood cDC2s (9, 32). Data suggest that murine LC development is dependent on CSF1R signaling (10, 11, 33), but limited data are available on its expression and function in human LCs. We report here that CSF1R was expressed by human LCs and was involved in LC migration toward CSF1. CSF1R stained LCH cells and TAMs, whereas CSF1 was abundantly produced in neoplastic tissues. CSF1R was expressed in normal LCs, tumor-associated LCs infiltrating skin cancer, and nodal LCs within the lymphatic sinuses of dermatopathic lymphadenitis. On the contrary, most dermal myeloid DCs, including a minor subset of CD207$^+$, lacked CSF1R. We demonstrated surface CSF1R on LCs isolated from human skin and on immature LCs *in vitro* generated from CD34$^+$ progenitors, CD14$^+$ monocytes, and BDCA1$^+$ cells, by using published protocols (32, 34).

The role of tumor-associated LCs has been partially investigated in skin cancer (35). Based on our study, CSF1-producing tumors might modulate the LC contexture at different sites, particularly in lymph nodes draining skin cancer. Similar to TAMs (7, 36), LCs might represent a relevant cell target during therapeutic CSF1R blockade. This hypothesis is further strengthened by our observation that CSF1R signaling was involved in LC expansion from CD34$^+$ precursors, suggesting that CSF1R blockade could result in a more dramatic and stable defect of the LC pool in these patients. We found that the presence of CSF1 during CD34$^+$ differentiation gave rise to a higher fraction of CD1a$^+$CD207$^+$ LCs that was reduced by CSF1R blockade. Our study corroborates previous observations (29, 37) on the role of

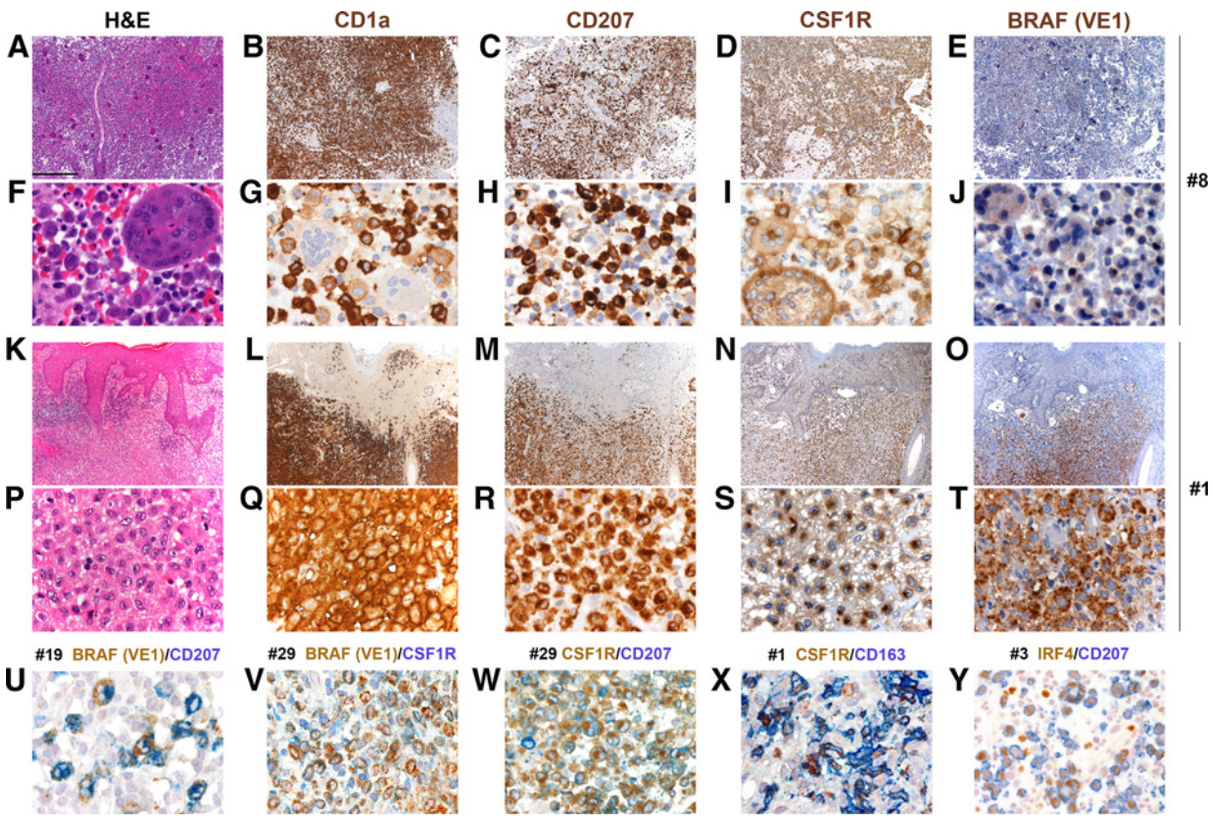

Figure 5.

CSF1R expression in LCH. Sections are from five human LCH and stained as labeled. Phenotypical characterization of two LCH (**A–T**), *BRAF*^{V600} (**A–J**), and *BRAF*^{V600E} (**K–T**) as defined by VE1 stain and digital PCR. Neoplastic cells, recognized by double stain for VE1 and CD207 (**U**), coexpress CSF1R (**V** and **W**). In the LCH microenvironment, CSF1R is also expressed on CD163$^+$ macrophages (**X**). A representative LCH case showing coexpression of CD207$^+$ and IRF4$^+$ in neoplastic cells is reported in **Y**. Sections are counterstained with hematoxylin. Original magnification: 40x (**A–E** and **K–O**: scale bar, 500 μm), 400x (**F–J**, **P–T**, **U**, **V**, **X**, and **Y**: scale bar, 50 μm), and 600x (**W**: scale bar, 33 μm). H&E, hematoxylin and eosin.

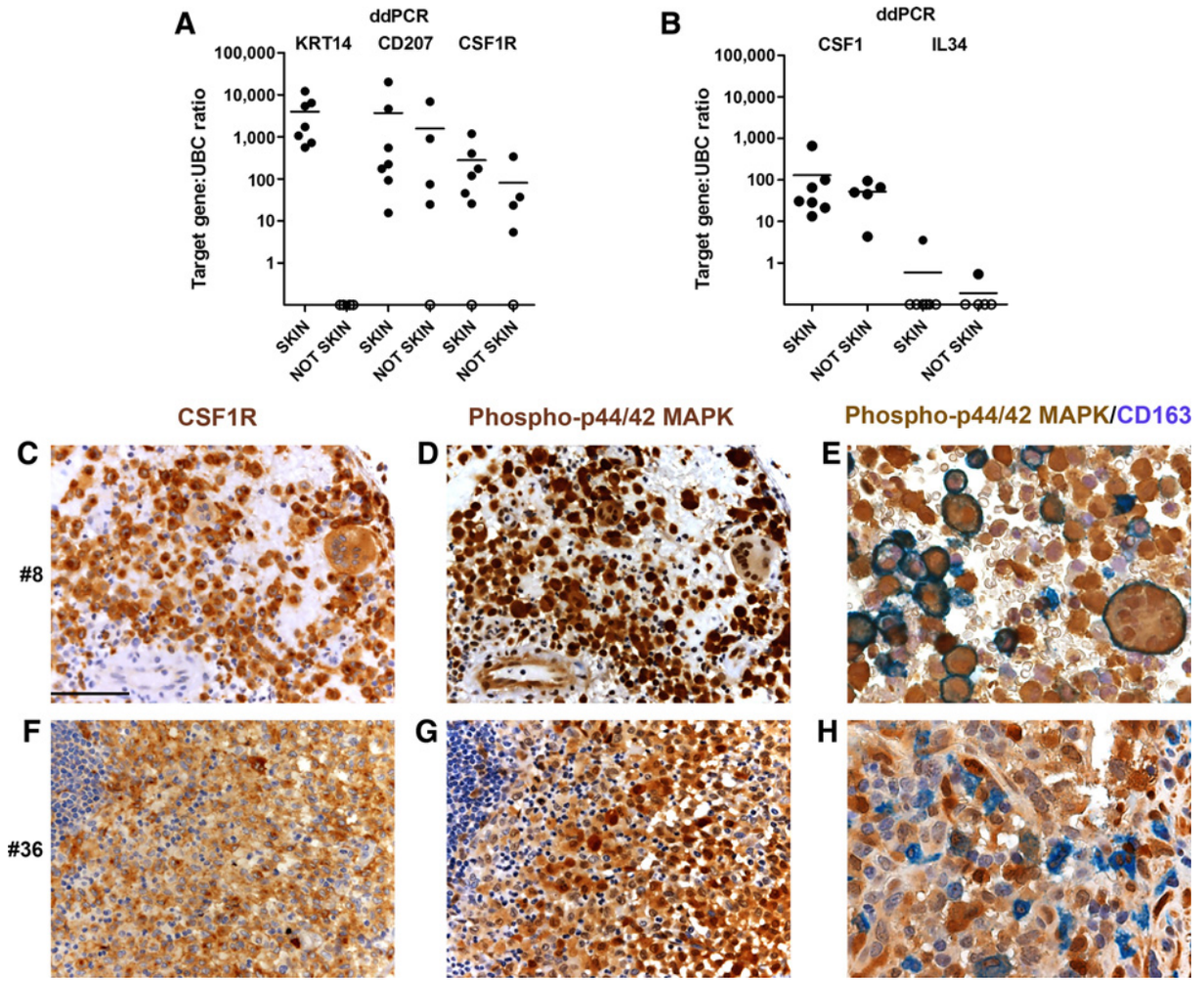

Figure 6.

CSF1R, CSF1, IL34 mRNA, and phospho-p44/42 MAPK (Thr202/Tyr204) in LCH tissue. The graphs illustrate the ddPCR-based detection of mRNA of KRT14, CD207, and CSF1R (**A**), as well as CSF1 and IL34 (**B**) in 12 LCH samples from cutaneous ($n = 7$) and extracutaneous ($n = 5$) sites. All samples were normalized to UBC mRNA expression. Undetectable mRNA is reported as 0.01. Sections are from two *BRAF*–wild-type LCH cases (#8 **C–E**, #36 **F–H**) and stained as labeled. On serial sections, LCH cells stained for anti–phospho-p44/42 MAPK (Thr202/Tyr204; **C** and **D** and **F** and **G**); the latter marker is also observed in a fraction of surrounding TAMs (**E** and **H**) as documented by staining for CD163. Sections are counterstained with hematoxylin. Original magnification: 200x (**C**, **D**, **F**, and **G**: scale bar, 100 μm) and 400x (**E** and **H**: scale bar, 50 μm).

CSF1 on the LC differentiation. We have not monitored LC precursors at various stage of differentiation during CSF1 culture and CSF1R blockade. However, it is known that $CD1a^{-}CD14^{+}CSF1R^{+}$ LC precursors require exogenous TGFβ (38). In addition, monocyte and DC progenitor cells express CSF1R (13). The effect of CSF1 and CSF1R blockage in LCs will certainly benefit from additional preclinical modeling and clinical monitoring on patients with cancer.

After receiving local signal, LCs migrate to draining lymph nodes. A set of proinflammatory stimuli and chemokines are required for LC migration to the nodal paracortex in the form of LC-derived $S100^{+}CD1a^{+}CD207^{+/-}$ IDCs. We found that CSF1R is expressed by immature LCs confined to the nodal sinuses, but it is rapidly downregulated upon maturation; in line with this observation, downregulation of CSF1R was documented in DCs exposed to TNF (39). In contrast with LCs, most IDCs lacked expression of CSF1R. Lack of CSF1R on IDCs could be a function of their mature phenotype, as demonstrated in this study. Alternatively, a non-LC identity has been proposed for IDCs (23), and other studies have demonstrated a cDC2 phenotype of IDCs (23). We found that a fraction of IDCs, particularly those located in the outer paracortex, mainly display a mature cDC2 phenotype, whereas IDCs in the inner paracortex more likely correspond to mature LCs.

In the current study, the expression of CSF1R in LCH biopsies was demonstrated by using two antibodies recognizing different CSF1R domains, and CSF1R reactivity was detected on LCH cells and TAMs. In *BRAF*–wild-type cases, $CSF1R^{+}$ cells coexpressed phospho-p44/42, suggesting CSF1R-dependent persistent activation of the MAPK pathway (28). Subcellular distribution of CSF1R in LCH cells included cytoplasmic and membrane localization. The observed subcellular heterogeneity may be consistent with the receptor compartmentalization during activation and subsequent degradation (40, 41). Alternatively, genomic abnormalities at the CSF1R locus or

posttranscriptional modification occurring in LCH cells, as observed in other cancers, might explain this variability (42).

IL34 was identified as an alternative ligand of CSF1R showing overlapping functions with CSF1 with respect to myeloid lineage differentiation, proliferation, and survival (43). Of note, we found that CSF1 was a potent chemoattractant for LCs, whereas IL34 showed no activity. These results support the notion that the two cytokines are partially redundant, as demonstrated by their different ability to induce morphologic changes and cytokines production in macrophages (44). Previous data confirm the role of CSF1R signaling in the chemotaxis of mononuclear phagocytes (45). CSF1 is highly expressed in carcinomas and sarcomas from different primary sites (46), whereas no data are available on LCH biopsies. We found that in contrast with IL34, CSF1 is abundantly produced in cutaneous and extracutaneous LCH tissue. This finding might explain the high serum concentration of CSF1 in patients with multisystemic LCH (16, 17) and suggests that $CSF1R^+$ LCH cells are recruited to neoplastic tissues by high local amounts of CSF1, as also reported in diffuse-type tenosynovial giant cell tumor (47).

Reports on systemic LCH indicate a hematopoietic origin of LCH cells. Clonal circulating precursors can be detected in the form of $CD34^+$ progenitors, monocytes, and cDC2s (5, 6), likely representing immediate precursors of LCH cells (22). High serum concentrations of TGFβ and CSF1 have been found in patients with LCH, suggesting their contribution in the differentiation of tissue-infiltrating neoplastic LCs from hematopoietic precursors (48). Transcriptomic studies revealed a monocyte-LC signature for LCH cells driven by JAG2-mediated activation of Notch (49). We observed a hybrid phenotype of $BRAF^{V600E}$ LCH cells, with cDC2 markers ($BDCA1^+$ and $IRF4^+$) admixed to LC markers (CD1a, CD207, and CSF1R) indicating that a partial LC commitment of cDC2 circulating precursors might also occur. Because CSF1R is required for terminal LC differentiation from CD34 precursors, as shown in the current study, we propose that CSF1R blockade might improve the LCH evolution.

In conclusion, although we recognize that additional data on fresh LCH cells are required to confirm our findings, we propose that LCH cases (and likely other LC/macrophage-derived neoplasms) might derive benefit from CSF1R blockade, a hypothesis suggested previously on preliminary findings (9). The relevance of this recommendation is further strengthened by the identification of activating CSF1R mutations in histiocytic neoplasm, with mutated tumor cells resulting in being sensitive to CSF1R blockade (18, 50). We envisage a synergistic clinical benefit by targeting tissue LCH cells (and their circulating precursors) and TAMs. Of note, CSF1R expression is also detected in the $BRAF^{V600E}$-mutated forms of LCH, a candidate group for BRAF inhibitors (51, 52) as a treatment option (53). However, the clinical benefit of MAPK inhibition in these patients is transient with frequent relapse (54–56), suggesting that additional treatment options are required for life-threatening LCH. Responders to CSF1R blockade will be likely enriched in the *BRAF*–wild-type subgroup. However, concomitant or sequential combination of BRAF and CSF1R blockade could be effective in $BRAF^{V600E}$ LCH, as observed in preclinical models of melanomas (57, 58), although it remains to be established how these compounds cooperate in LCH.

Disclosure of Potential Conflicts of Interest

No potential conflicts of interest were disclosed.

Authors' Contributions

Conception and design: T. Musso, W. Vermi

Development of methodology: S. Lonardi, S. Scutera, S. Licini, L. Benerini Gatta, D. Bollero, M. Tomaselli, D. Medicina

Acquisition of data (provided animals, acquired and managed patients, provided facilities, etc.): S. Scutera, L. Lorenzi, A.M. Cesinaro, C. Castagnoli, D. Bollero, R. Sparti, F. Calzetti, F. Facchetti

Analysis and interpretation of data (e.g., statistical analysis, biostatistics, computational analysis): S. Lonardi, S. Scutera, R. Sparti, M.A. Cassatella, T. Musso, W. Vermi

Writing, review, and/or revision of the manuscript: S. Lonardi, S. Scutera, L. Lorenzi, M.A. Cassatella, F. Facchetti, T. Musso, W. Vermi

Administrative, technical, or material support (i.e., reporting or organizing data, constructing databases): S. Lonardi, A.M. Cesinaro

Study supervision: T. Musso, W. Vermi

Acknowledgments

The authors greatly appreciate the help from Dr. Carola Ries by reading this article and providing excellent comments. The authors are grateful to Fondazione Beretta (Brescia, Italy) for support to S. Lonardi, M. Tomaselli, and S. Licini. The authors thank the pathologists, technicians, clinicians, nurses, and administrative employers who have provided support to the study and for the follow-up of patients with LCH. The authors acknowledge AIRC (Associazione Italiana per la Ricerca sul Cancro) Foundation for its financial support (IG 15378-2014 and IG 23179; to W. Vermi). The authors are grateful to Mattia Bugatti for his excellent support on preparation of human tissue biopsies.

The costs of publication of this article were defrayed in part by the payment of page charges. This article must therefore be hereby marked *advertisement* in accordance with 18 U.S.C. Section 1734 solely to indicate this fact.

Received April 1, 2019; revised December 5, 2019; accepted March 25, 2020; published first April 1, 2020.

References

1. Haroche J, Cohen-Aubart F, Rollins BJ, Donadieu J, Charlotte F, Idbaih A, et al. Histiocytoses: emerging neoplasia behind inflammation. Lancet Oncol 2017;18:e113–e25.
2. Haupt R, Minkov M, Astigarraga I, Schafer E, Nanduri V, Jubran R, et al. Langerhans cell histiocytosis (LCH): guidelines for diagnosis, clinical work-up, and treatment for patients till the age of 18 years. Pediatr Blood Cancer 2013;60:175–84.
3. Diamond EL, Durham BH, Haroche J, Yao Z, Ma J, Parikh SA, et al. Diverse and targetable kinase alterations drive histiocytic neoplasms. Cancer Discov 2016;6:154–65.
4. Sahm F, Capper D, Preusser M, Meyer J, Stenzinger A, Lasitschka F, et al. BRAFV600E mutant protein is expressed in cells of variable maturation in Langerhans cell histiocytosis. Blood 2012;120:e28–34.
5. Berres ML, Lim KP, Peters T, Price J, Takizawa H, Salmon H, et al. BRAF-V600E expression in precursor versus differentiated dendritic cells defines clinically distinct LCH risk groups. J Exp Med 2015;212:281.
6. Durham BH, Roos-Weil D, Baillou C, Cohen-Aubart F, Yoshimi A, Miyara M, et al. Functional evidence for derivation of systemic histiocytic neoplasms from hematopoietic stem/progenitor cells. Blood 2017;130:176–80.
7. Ries CH, Cannarile MA, Hoves S, Benz J, Wartha K, Runza V, et al. Targeting tumor- associated macrophages with anti-CSF-1R antibody reveals a strategy for cancer therapy. Cancer Cell 2014;25:846–59.
8. Micheletti A, Finotti G, Calzetti F, Lonardi S, Zoratti E, Bugatti M, et al. slan/M-DC8+ cells constitute a distinct subset of dendritic cells in human tonsils. Oncotarget 2016;7:161–75.

9. Ginhoux F, Tacke F, Angeli V, Bogunovic M, Loubeau M, Dai XM, et al. Langerhans cells arise from monocytes in vivo. Nat Immunol 2006;7:265–73.
10. Wang Y, Szretter KJ, Vermi W, Gilfillan S, Rossini C, Cella M, et al. IL-34 is a tissue- restricted ligand of CSF1R required for the development of Langerhans cells and microglia. Nat Immunol 2012;13:753–60.
11. Greter M, Lelios I, Pelczar P, Hoeffel G, Price J, Leboeuf M, et al. Stroma-derived interleukin-34 controls the development and maintenance of Langerhans cells and the maintenance of microglia. Immunity 2012;37:1050–60.
12. Bigley V, McGovern N, Milne P, Dickinson R, Pagan S, Cookson S, et al. Langerin-expressing dendritic cells in human tissues are related to CD1c+ dendritic cells and distinct from Langerhans cells and CD141high XCR1+ dendritic cells. J Leukoc Biol 2015;97:627–34.
13. Breton G, Lee J, Zhou YJ, Schreiber JJ, Keler T, Puhr S, et al. Circulating precursors of human CD1c+ and CD141+ dendritic cells. J Exp Med 2015;212: 401–13.
14. Calzetti F, Tamassia N, Micheletti A, Finotti G, Bianchetto-Aguilera F, Cassatella MA. Human dendritic cell subset 4 (DC4) correlates to a subset of CD14(dim/-) CD16(++) monocytes. J Allergy Clin Immunol 2018;141:2276–9.
15. Kashem SW, Haniffa M, Kaplan DH. Antigen-presenting cells in the skin. Annu Rev Immunol 2017;35:469–99.
16. Rolland A, Guyon L, Gill M, Cai YH, Banchereau J, McClain K, et al. Increased blood myeloid dendritic cells and dendritic cell-poietins in Langerhans cell histiocytosis. J Immunol 2005;174:3067–71.
17. Morimoto A, Oh Y, Nakamura S, Shioda Y, Hayase T, Imamura T, et al. Inflammatory serum cytokines and chemokines increase associated with the disease extent in pediatric Langerhans cell histiocytosis. Cytokine 2017;97: 73–9.
18. Durham BH, Lopez-Rodrigo E, Abramson DH, Picarsic J, Pastore A, Mandelker D, et al. Activating mutations in CSF1R and additional receptor tyrosine kinases in sporadic and familial histiocytic neoplasms. Blood 2018;132:1.
19. Martin-Moreno AM, Roncador G, Maestre L, Mata E, Jimenez S, Martinez-Torrecuadrada JL, et al. CSF1R protein expression in reactive lymphoid tissues and lymphoma: its relevance in classical hodgkin lymphoma. PLoS One 2015;10: e0125203.
20. Vermi W, Bonecchi R, Facchetti F, Bianchi D, Sozzani S, Festa S, et al. Recruitment of immature plasmacytoid dendritic cells (plasmacytoid monocytes) and myeloid dendritic cells in primary cutaneous melanomas. J Pathol 2003;200:255–68.
21. Milne P, Bigley V, Gunawan M, Haniffa M, Collin M. CD1c+ blood dendritic cells have Langerhans cell potential. Blood 2015;125:470–3.
22. Milne P, Bigley V, Bacon CM, Neel A, McGovern N, Bomken S, et al. Hematopoietic origin of langerhans cell histiocytosis and Erdheim-Chester disease in adults. Blood 2017;130:167–75.
23. Collin M, Bigley V. Human dendritic cell subsets: an update. Immunology 2018; 154:3–20.
24. Kissenpfennig A, Henri S, Dubois B, Laplace-Builhe C, Perrin P, Romani N, et al. Dynamics and function of Langerhans cells in vivo: dermal dendritic cells colonize lymph node areas distinct from slower migrating Langerhans cells. Immunity 2005;22:643–54.
25. Boulakirba S, Pfeifer A, Mhaidly R, Obba S, Goulard M, Schmitt T, et al. IL-34 and CSF-1 display an equivalent macrophage differentiation ability but a different polarization potential. Sci Rep 2018;8:256.
26. El-Gamal MI, Anbar HS, Yoo KH, Oh CH. FMS kinase inhibitors: current status and future prospects. Med Res Rev 2013;33:599–636.
27. Jones GE, Prigmore E, Calvez R, Hogan C, Dunn GA, Hirsch E, et al. Requirement for PI 3- kinase gamma in macrophage migration to MCP-1 and CSF-1. Exp Cell Res 2003;290:120–31.
28. Stanley ER, Chitu V. CSF-1 receptor signaling in myeloid cells. Cold Spring Harb Perspect Biol 2014;6. pii: a021857.
29. Mollah ZU, Aiba S, Nakagawa S, Hara M, Manome H, Mizuashi M, et al. Macrophage colony-stimulating factor in cooperation with transforming growth factor-beta1 induces the differentiation of CD34+ hematopoietic progenitor cells into Langerhans cells under serum-free conditions without granulocyte-macrophage colony-stimulating factor. J Invest Dermatol 2003;120:256–65.
30. Strobl H, Bello-Fernandez C, Riedl E, Pickl WF, Majdic O, Lyman SD, et al. flt3 ligand in cooperation with transforming growth factor-beta1 potentiates in vitro development of Langerhans-type dendritic cells and allows single-cell dendritic cell cluster formation under serum-free conditions. Blood 1997;90:1425–34.
31. Geissmann F, Lepelletier Y, Fraitag S, Valladeau J, Bodemer C, Debre M, et al. Differentiation of langerhans cells in langerhans cell histiocytosis. Blood 2001;97: 1241–8.
32. Martinez-Cingolani C, Grandclaudon M, Jeanmougin M, Jouve M, Zollinger R, Soumelis V. Human blood BDCA-1 dendritic cells differentiate into Langerhans-like cells with thymic stromal lymphopoietin and TGF-beta. Blood 2014; 124:2411–20.
33. Wang Y, Bugatti M, Ulland TK, Vermi W, Gilfillan S, Colonna M. Nonredundant roles of keratinocyte-derived IL-34 and neutrophil-derived CSF1 in Langerhans cell renewal in the steady state and during inflammation. Eur J Immunol 2016;46: 552–9.
34. Hoshino N, Katayama N, Shibasaki T, Ohishi K, Nishioka J, Masuya M, et al. A novel role for Notch ligand Delta-1 as a regulator of human Langerhans cell development from blood monocytes. J Leukoc Biol 2005;78:921–9.
35. Atmatzidis DH, Lambert WC, Lambert MW. Langerhans cell: exciting developments in health and disease. J Eur Acad Dermatol Venereol 2017; 31:1817–24.
36. Ries CH, Hoves S, Cannarile MA, Ruttinger D. CSF-1/CSF-1R targeting agents in clinical development for cancer therapy. Curr Opin Pharmacol 2015;23:45–51.
37. Takashima A, Edelbaum D, Kitajima T, Shadduck RK, Gilmore GL, Xu S, et al. Colony- stimulating factor-1 secreted by fibroblasts promotes the growth of dendritic cell lines (XS series) derived from murine epidermis. J Immunol 1995; 154:5128–35.
38. Caux C, Vanbervliet B, Massacrier C, Dezutter-Dambuyant C, de Saint-Vis B, Jacquet C, et al. CD34+ hematopoietic progenitors from human cord blood differentiate along two independent dendritic cell pathways in response to GM-CSF+TNF alpha. J Exp Med 1996;184:695–706.
39. Chomarat P, Banchereau J, Davoust J, Palucka AK. IL-6 switches the differentiation of monocytes from dendritic cells to macrophages. Nat Immunol 2000;1: 510–4.
40. Rohde CM, Schrum J, Lee AW. A juxtamembrane tyrosine in the colony stimulating factor-1 receptor regulates ligand-induced Src association, receptor kinase function, and down-regulation. J Biol Chem 2004;279:43448–61.
41. Xiong Y, Song D, Cai Y, Yu W, Yeung YG, Stanley ER. A CSF-1 receptor phosphotyrosine 559 signaling pathway regulates receptor ubiquitination and tyrosine phosphorylation. J Biol Chem 2011;286:952–60.
42. Soares MJ, Pinto M, Henrique R, Vieira J, Cerveira N, Peixoto A, et al. CSF1R copy number changes, point mutations, and RNA and protein overexpression in renal cell carcinomas. Mod Pathol 2009;22:744–52.
43. Droin N, Solary E. Editorial: CSF1R, CSF-1, and IL-34, a "menage a trois" conserved across vertebrates. J Leukoc Biol 2010;87:745–7.
44. Chihara T, Suzu S, Hassan R, Chutiwitoonchai N, Hiyoshi M, Motoyoshi K, et al. IL-34 and M-CSF share the receptor Fms but are not identical in biological activity and signal activation. Cell Death Differ 2010;17:1917–27.
45. Pixley FJ, Stanley ER. CSF-1 regulation of the wandering macrophage: complexity in action. Trends Cell Biol 2004;14:628–38.
46. Laoui D, Van Overmeire E, De Baetselier P, Van Ginderachter JA, Raes G. Functional relationship between tumor-associated macrophages and macrophage colony- stimulating factor as contributors to cancer progression. Front Immunol 2014;5:489.
47. West RB, Rubin BP, Miller MA, Subramanian S, Kaygusuz G, Montgomery K, et al. A landscape effect in tenosynovial giant-cell tumor from activation of CSF-1 expression by a translocation in a minority of tumor cells. Proc Natl Acad Sci U S A 2006;103:690–5.
48. Carrera Silva EA, Nowak W, Tessone L, Olexen CM, Ortiz Wilczynski JM, Estecho IG, et al. CD207(+)CD1a(+) cells circulate in pediatric patients with active Langerhans cell histiocytosis. Blood 2017;130:1898–902.
49. Schwentner R, Jug G, Kauer MO, Schnoller T, Waidhofer-Sollner P, Holter W, et al. JAG2 signaling induces differentiation of CD14(+) monocytes into Langerhans cell histiocytosis-like cells. J Leukoc Biol 2019;105:101–11.
50. Durham BH, Lopez Rodrigo E, Picarsic J, Abramson D, Rotemberg V, De Munck S, et al. Activating mutations in CSF1R and additional receptor tyrosine kinases in histiocytic neoplasms. Nat Med 2019;25:1839–42.
51. Chakraborty R, Hampton OA, Shen X, Simko SJ, Shih A, Abhyankar H, et al. Mutually exclusive recurrent somatic mutations in MAP2K1 and BRAF support a central role for ERK activation in LCH pathogenesis. Blood 2014;124:3007–15.
52. Haroche J, Cohen-Aubart F, Emile JF, Maksud P, Drier A, Toledano D, et al. Reproducible and sustained efficacy of targeted therapy with vemurafenib in patients with BRAF(V600E)-mutated Erdheim-Chester disease. J Clin Oncol 2015;33:411–8.
53. Diamond EL, Subbiah V, Lockhart AC, Blay JY, Puzanov I, Chau I, et al. Vemurafenib for BRAF V600-mutant erdheim-chester disease and langerhans

cell histiocytosis: analysis of data from the histology-independent, phase 2, open-label VE-BASKET study. JAMA Oncol 2018;4:384–8.
54. Azorsa DO, Lee DW, Wai DH, Bista R, Patel AR, Aleem E, et al. Clinical resistance associated with a novel MAP2K1 mutation in a patient with Langerhans cell histiocytosis. Pediatr Blood Cancer 2018;65:e27237.
55. Gandolfi L, Adamo S, Pileri A, Broccoli A, Argnani L, Zinzani PL. Multisystemic and multiresistant langerhans cell histiocytosis: a case treated with BRAF inhibitor. J Natl Compr Canc Netw 2015;13:715–8.
56. Donadieu J, Larabi IA, Tardieu M, Visser J, Hutter C, Sieni E, et al. Vemurafenib for refractory multisystem langerhans cell histiocytosis in children: an international observational study. J Clin Oncol 2019;37:2857–65.
57. Giricz O, Mo Y, Dahlman KB, Cotto-Rios XM, Vardabasso C, Nguyen H, et al. The RUNX1/IL-34/CSF-1R axis is an autocrinally regulated modulator of resistance to BRAF-V600E inhibition in melanoma. JCI Insight 2018;3. pii: 120422.
58. Ngiow SF, Meeth KM, Stannard K, Barkauskas DS, Bollag G, Bosenberg M, et al. Co-inhibition of colony stimulating factor-1 receptor and BRAF oncogene in mouse models of BRAF(V600E) melanoma. Oncoimmunology 2016;5:e1089381.